

Gas Sensor with Nanostructured Oxide Semiconductor Materials

Ghim Wei Ho

*Department of Electrical and Computer Engineering, National University of Singapore,
 4 Engineering Drive 3, Singapore 117576*

Metal oxides are often the choice for conductometric gas sensing due to their thermal and environmental stability as well as good response reversibility. Due to the fact that sensing with these materials relies on interactions with the surface, one strategy to enhance the sensitivity is to increase the surface area or active sites by decreasing their physical dimensions. Nanoscale metal oxides such as nanoparticles, nanospheres, nanotubes, nanobelts and nanowires are routinely synthesized for development of solid-state gas sensors with improved sensing properties. In this review, gas sensing applications of a variety of metal oxide nanostructures in various device configurations; bulk, two-terminal and field effect transistor (FET) sensors are presented. The application of nanostructures as building blocks for sensor can be achieved by implementing effective assembly and integration techniques to transfer the nanostructures from growth substrates onto their respective device substrates. Two common methods have been reviewed which include transfer printing and dielectrophoretic alignment of nanowires. In essence, these approaches employ external forces to align the nanostructures via dry and wet media respectively. Finally, the non conventional substrate sensors such as textile and free standing nanowire sheet are reviewed. The non conventional substrates have the advantages of being flexible, shock proof, wearable and portable etc.

Keywords: Metal Oxides, Sensors, Nanowires, Alignment, Field Effect Transistor.

CONTENTS

1. Introduction	150
2. Nanostructure Sensors	152
2.1. Bulk Nanostructure Sensor	152
2.2. Two-Terminal Thin Film Nanostructure Sensor	154
2.3. FET Nanostructure Sensor	157
3. Directed Assembly of Nanostructure Sensors	160
3.1. Transfer Printed Nanostructure Sensor	160
3.2. Dielectrophoretic Assembled Nanostructure Sensor	161
4. Non-Conventional Substrate Sensor	163
4.1. Textile Sensor	165
4.2. Free Standing Sheet Sensor	166
5. Conclusions	166
6. Future Directions	166
Acknowledgments	167
References and Notes	167

1. INTRODUCTION

There is a great demand to enhance the sensitivity of chemical sensors for various sensing applications such as monitoring and conditioning of air quality, detection of flammable or toxic gases, medical diagnosis, detection of chemical-warfare agents, and optimization of combustion

efficiency in automobile engines. Thus, the quality of gas sensors has a great impact in many areas such as environmental, domestic, public, automotive safety and security. There are three broad types of gaseous species that are often monitored and detected:

- Toxic gas species (CO, SO₂, NO_x etc.)
- Corrosive species (Cl₂, F₂, HF etc.)
- Explosive species (CH₄, hydrocarbons, nitrous compounds etc.).

Toxic gases are essentially being monitored in cities and homes, the corrosive gasses are monitored in chemical petrochemical and food industries and finally the explosive species are associated to public security.

A typical sensor consists of three main parts: (i) sensing material where the molecular recognition or chemical reactions take place, (ii) transducer which serves as an interface between the sensor and environment and transforms the molecular adsorption and/or chemical reactions into some physical parameters and (iii) signal processor system to quantify the physical parameter and feed the information back into a readable output.

Sensors can be classified into various transducing principles.¹ The types of transducers include (i) electrical

(or electrochemical) transducers, which transform chemical reactions into electrical signals—either current (amperometric sensors), or voltage (potentiometric) (ii) gravimetric transducers which register changes in mass due to molecular adsorption and (iii) optical transducers which are based on different interferometry measure changes in refractive index and thickness of membranes caused by different chemical reactions. To realize a superior solid-state gas sensor, three well-known “S” which is the sensitivity, selectivity and stability of a sensor are often studied and improved.

The sensitivity (S) of a sensor is defined as,

$$S = \frac{dy}{dx}$$

the ability to detect a given analyte concentration which is usually determined from a slope of an output signal y (e.g., a change in the electrical resistance) for a given concentration x of a specific gas to be detected.^{2,3}

The selectivity (Q) of a sensor,

$$Q(\%) = 100 \times \frac{dy/dx'}{dy/dx}$$

is the ability to discriminate between a mixture of gases which is defined by the cross sensitivity to all other gases.^{2,3}

Oxide materials represent an important class of materials whose properties cover the entire range from insulators, semiconductors to metal. In addition, oxide materials possess a broad range of electronic, chemical, and physical properties that are often highly sensitive to the changes in a chemical environment, through a variety of detection and transduction principles, based on the semiconducting, ionic conducting, photoconducting, piezoelectric, pyroelectric, and luminescence properties.⁴⁻⁸

Thus, the interest for gas-sensing applications of oxide materials is continuously growing, and further development of this field will require a constant effort towards the synthesis and processing of nanomaterials suitable for specified applications. Theoretically, there is no limitation for the use of any oxide materials for gas sensing

applications. However, not all oxide materials are effective sensors. The selection of optimal sensing material is highly dependent on the design, manufacturing, chemical activity, stability etc. Because of the wide availability of synthesis and processing of oxides materials, a careful selection of methodology to prepare oxide of sufficiently fine dispersion, porous structure, high crystallinity and bulk quantity is preferred. Nevertheless, novel synthesis and fabrication techniques as well as new material science and physics await discovery and remain to be explored based on the newly acquired nanoscience and nanotechnology knowledge. At present, various nanocrystalline oxide nanomaterial such as indium oxide (In_2O_3), titanium dioxide (TiO_2), gallium oxide (Ga_2O_3), zinc oxide (ZnO), tin oxide (SnO_2), tungsten oxide (WO_3) etc. are synthesized for gas sensing applications.⁹⁻¹⁴ Some information and operating parameters about the commonly employed solid-state oxide gas sensing materials characteristics are summarized in the Table I.

Nanocrystalline oxide materials are classified into different categories depending on their dimensions and structures. Numerous oxide nanostructures of zero, one and two-dimensional oxide nanostructures with suitable properties, composition and morphologies are routinely being synthesized for gas sensing applications. The synthetic conditions to obtain nanocrystalline oxides product are extremely broad, ranging from high temperatures and/or pressures coupled with long processing times, to very mild conditions without any applied pressure and even at room temperature. Such a large variation of synthetic conditions is a result of the large variety of reactions available in the formation of crystalline structures. Generally, there are two methods of preparing oxide nanostructures namely the physical (dry) and chemical (wet) techniques. The physical techniques include chemical vapor deposition, thermal vapor deposition, solid-state reaction, sputtering etc. starting from oxide powder, oxide target, inert gas to various reactive gasses. The main structures that are synthesized via physical methods are thin films, nanowires, nanotubes etc. On the other hand, chemical techniques include sol-gel, hydro/solvothermal, electrodeposition, Langmuir-Blodgett etc. starting from various



Ghim Wei Ho is an assistant professor of Electrical and Computer Engineering in National University of Singapore. She received her Ph.D. degree in Engineering from Nanoscience Centre, University of Cambridge in 2006, M.Sc. and B.Sc. from National University of Singapore in 2001. She is first in the world to develop novel SiC nanoflowers and multi-coaxial nanowires with media TV coverage in NBC, ScienCentral and BBC News, UK and many newspaper coverages in Daily Telegraphy, Cambridge Evening Newspaper, Streets. Her Nanoscience and Nanosystems group is focused on fundamental science of the physical and chemical processes of nanostructured materials synthesis, unique properties and nanosystems. The research focus involved the study of unique phenomena and manipulation of material at the nanoscale which revolves around the realization of solar cell, chemical sensor and drug delivery systems.

Table I. Properties and operating parameters on some of the commonly employed solid-state oxide gas sensing materials.

Metal oxide	Melting point	Type of conductivity	Operating temperature	Optimal gas detection	Stability	Humidity sensitivity
SnO ₂	1900–1930	<i>n</i>	200–400	CO, H ₂ , CH ₄	Excellent	High
Ga ₂ O ₃	1740–1805	<i>n</i>	400–1000	O ₂ , CO, NO ₂ , NH ₃	Good	Low
In ₂ O ₃	1910–2000	<i>n</i>	200–400	O ₃ , NO ₂ , NH ₃	Fair	Low
TiO ₂	1855	<i>n</i>	350–800	O ₂ , CO, SO ₂	Fair	Low
ZnO	1800–1975	<i>n</i>	250–350	CH ₄ , C ₄ H ₁₀ , O ₂ , NO ₂ , NH ₃	Fair	High
WO ₃	1470	<i>n</i>	200–500	O ₃ , N ₂ O, SO ₂ , H ₂ S	Excellent	Low

oxide precursors, solvents, surfactants and additives. The structures prepared by physical techniques have the advantages of being able to directly grow onto the final substrate and can be directly manipulated for the fabricating of a nanodevice. On the other hand, the advantages of producing nanostructured materials using chemical route is that large quantity of processable nanostructures can be obtained in a cost-effective, highly-scalable and mild reaction condition.

2. NANOSTRUCTURE SENSORS

Various oxide nanostructured materials are prepared and deposited as thick, thin film or incorporated into transistor for gas sensing applications.^{15–20} The sensor performance depends on percolation path of electrons through intergranular regions, thus by varying small details in the preparation process, each sensor differs slightly in its sensing characteristics. The first generation sensors are prepared by thick film technology starting from powder. Then comes along the thin film technology whereby physical deposition techniques are largely implemented. Thin films are developed based on vapor phase deposition using chemical vapor deposition, sputtering, evaporation etc. However, the sensing performances are still not satisfactory due to a relatively low surface area of the prepared thick and thin films. Another downside aspect of both the thin and thick films is the significant electrical properties drift due to grain coalescence, porosity modification and grain-boundary issues. These effects become especially critical when the metal oxide active layers are operated at relatively high temperature in order to guarantee the reversibility of chemical reactions at the surface. Thus, several solutions have been put forward; first to increase the surface area by synthesizing nanostructures and then to stabilize the nanostructure by e.g., addition of a foreign element or phase. Up to date, various types of dopants,²¹ such as group-III (Al,^{22,23} Ga,^{24,25} In²⁵), group-IV (Sn,^{25,26}), group-V (N,^{22,23} P,²⁷ As,^{28,29} Sb³⁰), group-VI (S³¹), and transition metal (Co,³² Fe,³³ Ni,³⁴ Mn³⁵) have been implanted into ZnO nanostructures. Doping group-III and IV elements into ZnO has proven to enhance its *n*-type conductivity.

More recently, a great step forward in the preparation of a highly stable and sensitive sensor has been made

by incorporating single crystal one-dimensional semiconducting oxides nanostructures (nanobelts, nanowires or nanoribbons) into the sensor.^{36–45} The high crystallinity and the nanosized lateral dimension assure improved stability and good sensing properties. Their novel phenomena and size effects make them interesting both for fundamental studies and for potential nanodevice applications, leading to a third generation of oxide gas sensors.

2.1. Bulk Nanostructure Sensor

The bulk nanostructure sensors that have been reported consist of nanostructures pressed into pellets,^{46–48} coated directly as thick film on ceramic tube or nanostructures grown on substrate and directly fabricated as sensors.^{49–54} Tan et al. have reported SnO₂ nanostructures pellet sensor where powders were processed into bulk sensor in a form of thick pellet (~1 mm).⁴⁸ Individual pellets were created by adding 0.5 g of the SnO₂ with embedded Pt wires and applying a pressure of 15 tons on a mould. The SnO₂ nanoparticles were prepared by solid-state reaction synthetic route whereby reactions are usually initiated by self-initiation via grinding. The solid-state reaction has several unique features: the reaction can be self-initiated at room temperature, and internally produced heat can be self-sustained to produce crystalline products (Figs. 1(a–d)). The effects of various reaction parameters are investigated to control the dimension of the SnO₂ nanoparticles which in turn were used for hydrogen sensing studies. Figure 1(e) shows that the SnO₂ nanostructure sensor exhibits highly consistent responses over many cycles, which translates to high device stability. Figure 1(f) shows the sensitivity–temperature relationships obtained for different average particle sizes of 20, 30 and 40 nm. It is observed that sensors made up of smaller nanoparticles possess higher gas sensitivities due to the increase in effective surface area.

Another type of bulk nanostructure sensors are based on thick film coating on ceramic tube incorporated with heater.^{55–57} Typically a ceramic tube is printed with metal electrodes and conducting wires (Fig. 2(a)). The working temperature of the sensor can be controlled by adjusting the heating voltage across a resistor inside the ceramic tube. A reference resistor is put in series with the sensor to form a complete measurement circuit. A working voltage was applied and by monitoring the output voltage across the reference resistor, the response of the sensor in air or in

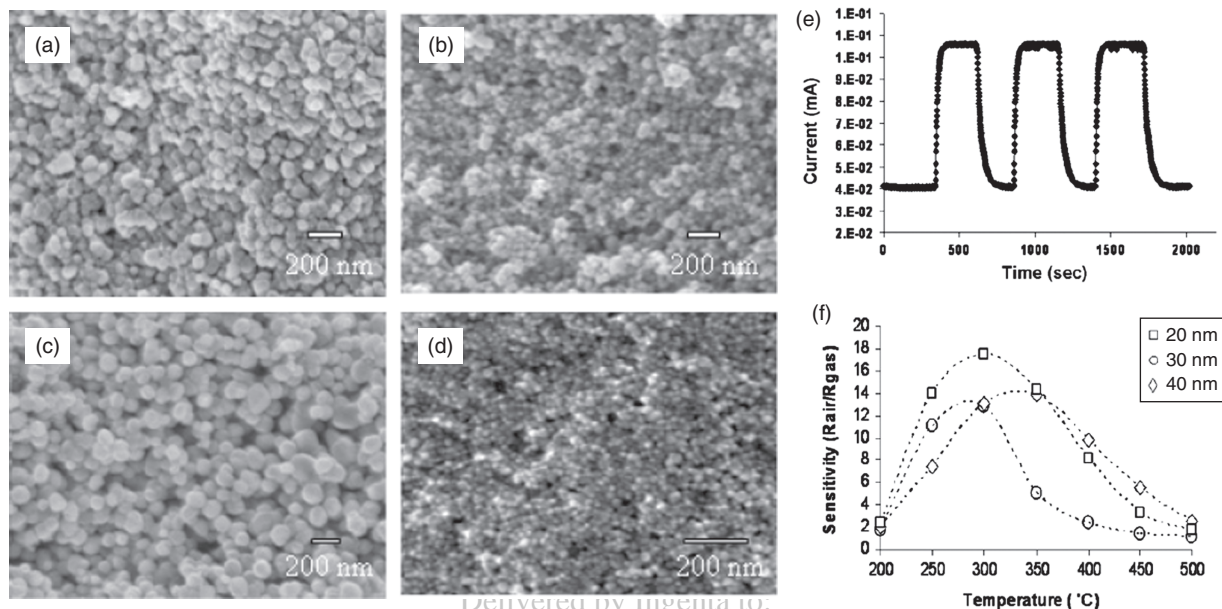


Fig. 1. SEM images of the SnO_2 nanostructures obtained with variation in (a–b) precursor and (c–d) additive concentrations. (e) Typical current response and (f) Sensitivity–temperature relationship of the bulk SnO_2 nanostructure hydrogen sensor. Reprinted with permission from [48], E. T. H. Tan et al., *Nanotechnology* 19, 255706, (2008). © 2008, IOP Publishing.

an analyte gas can be measured. Guo et al. have reported Fe_2O_3 porous nanorods and branched nanostructures bulk sensors. The nanostructures were synthesized by dehydration and recrystallisation of $\beta\text{-FeOOH}$ precursor, which was obtained from the hydrothermal reaction of FeCl_3 with urea in an aqueous system. The morphology of the as-prepared nanostructures was characterized by TEM as shown in Figure 2(b). The inset shows the electron diffraction pattern and ring which indicate the polycrystalline nature. Figure 2(c) shows voltage response of the sensor at a working temperature of 150°C and 30% relative humidity. It can be seen that output voltage values increased abruptly on the injection of ethanol and then decreased rapidly and recovered to their initial value after the test gas was released. The response and recovery time of the nanostructure-based sensors were 1–3 and 4–8 s, respectively. There is also work reported on Fe_2O_3 nanotubes which show good ethanol sensing performance.⁵⁸

Similarly, other bulk nanostructure sensor based on thick film coated on ceramic tube is also reported.⁵⁷ Homogeneous $\text{In}(\text{OH})_3$ or InOOH colloidal supernatant was coated onto a ceramic tube, on which a pair of Au electrodes was printed. After the solvent evaporation, the colloidal crystals form a thin film on the ceramic tube. Then, the ceramic tube was annealed at 300 and 400°C for 2 h to transform $\text{In}(\text{OH})_3$ or InOOH into cubic and hexagonal In_2O_3 respectively. The conductance undergoes a drastic rise upon the injection of reducing compound, ethanol and drops to its initial value after ethanol is released. These sensors show a quick response of less than 10 s and recovery time of 15 s. The lowest detection limit is down to 1 ppm. The

response of the sensor correlates to the concentration of the test gas, the structure and the morphology of In_2O_3 .

Another form of bulk nanostructure sensor is based on nanowire grown and fabricated directly on the substrate. From the viewpoint of device structure, the conventional nanowire-based gas sensors were fabricated either by pick-and-place process of a single nanowire followed by making electrical contacts to individual nanowire. The device fabrication process uses expensive and time consuming procedures of sonication and dispersal of nanowires on substrate with electrodes fabricated by electron-beam lithography. In this bulk nanowire sensor device, all these complicated processing steps can be eliminated. Figures 3(a–b) shows side and top-view SEM images of ZnO nanowires grown on patterned electrodes.⁵⁹ Figure 3(c) shows the schematic diagram of the bulk nanowire sensor device which was fabricated directly on the growth substrate. There are many nanowire-nanowire junctions (Fig. 3(d)) which act as electrical conducting path. Figure 3(e) shows the gas response as a function of NO_2 concentration at 225°C where the gas response is directly proportional to gas concentration. Figure 3(f) shows evidence of saturation at the NO_2 concentration larger than 3 ppm. This can be explained by the competition between the adsorption sites versus the concentration of target gas. In a low gas concentration, the available adsorption sites on the surface of ZnO can be regarded as infinite compared with the NO_2 concentration, and thus the rate-determining step might be the surface reaction between NO_2 molecules and ZnO surface. Thus surface reactions are linearly dependent on the NO_2 concentration as long as adsorption sites are enough.

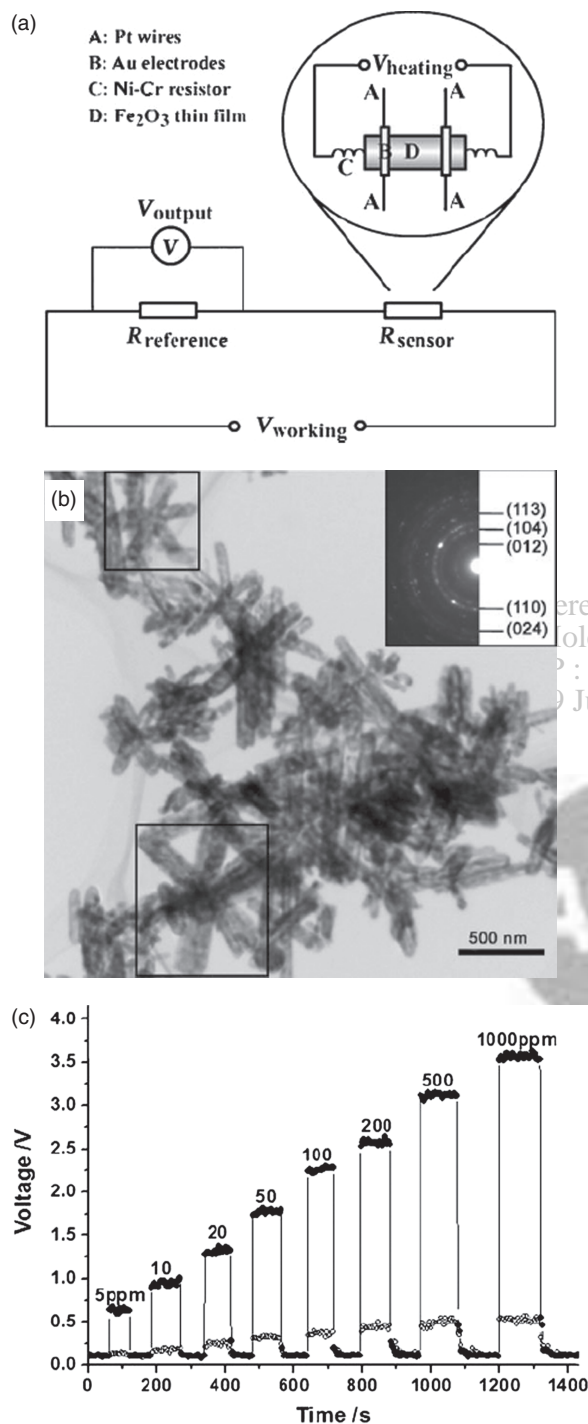


Fig. 2. (a) Schematic illustration of the gas sensor measurement system. (b) TEM images of the as-synthesized Fe_2O_3 nanostructures. (c) Real-time ethanol sensing characteristics of sensors based on the prepared Fe_2O_3 nanostructures. Reprinted with permission from [55], X. L. Gou et al., *Chem. Eur. J.* 14, 5996 (2008). © 2008, Wiley.

Similarly, bulk nanowire sensors were fabricated directly on nanowires grown on substrates.⁶⁰ Contacts to the multiple nanowires network were formed using a shadow mask and sputtering of Al/Ti/Au electrodes. The sensor studies were on the time dependence of relative

resistance change of either metal-coated or uncoated network ZnO nanowire as the gas ambient is switched from N_2 to 500 ppm of H_2 in air and then back to N_2 . The highest response is Pt coated nanowires which is followed by Pd while the other metals produce little or no change in response. This is consistent with the known catalytic properties of these metals for hydrogen dissociation. The sensors response to various gas concentrations and it can detect <100 ppm H_2 . Other example of nanowire gas sensors which have been fabricated on Cd-Au comb-shaped interdigitating electrodes is shown in Figures 3(g–h).⁶¹ The bulk nanowire sensors maintain high response to hydrogen concentration in the range of 10 to 1000 ppm. This high response is attributed to the highly connected network of nanowires. Similarly, microtrench has been created on Si substrates and nanowires are grown using a thermal chemical vapor deposition and directly fabricated into sensor.⁶² SnO_2 nanowires are synthesized to be sufficiently long to bridge across trenched electrodes. In this process, complicated and individual alignment process is avoided and a number of devices can be fabricated in a single process step at a wafer scale. The gas-sensing characteristics of the developed sensor were significantly better when compared to other types of NO_2 sensors reported in the literature. The sensitivity was >150 at a NO_2 concentration of 5 ppm.

2.2. Two-Terminal Thin Film Nanostructure Sensor

Two terminal thin film sensor made up of one to few monolayer of nanostructures spanning across two electrodes are commonly fabricated. The sensing device consists of a low-density layer of nanostructures which are deposited/dispersed onto prepared coplanar electrodes. Ho et al. have reported on two-terminal mesoporous nanospheres thin film sensor (Fig. 4(a)).⁶³ The nanospheres (Figs. 4(b–c)) were synthesized based on a simple hydrothermal method using potassium stannate trihydrate as a precursor in an ethanol–deionized water mixed solvent. The parameters affecting the morphology and porosity of the synthesized SnO_2 nanostructures are investigated by varying various experimental conditions such as temperature, precursor concentration and additives. The nanospheres grown without urea additive and at higher temperature (225 °C) exhibit the highest specific surface area of 156.4 m^2/g with pore diameter of 5.3 nm. The nanospheres were diluted and dispersed in water before drop casting a few monolayers onto the electrodes. Figure 4(d) shows the current response graphs obtained by cycling it alternately in dry air and H_2 at various operating temperature. It is noted that the response time (90% of $R_{\text{air}}-R_{\text{gas}}$) is achieved within the first 1.3–3.0 min while the recovery time is 1.4–4.6 min, depending on the operating temperature of the sensor. The effect of operating temperature of the reference sample on the sensor performance is investigated. The responses of the

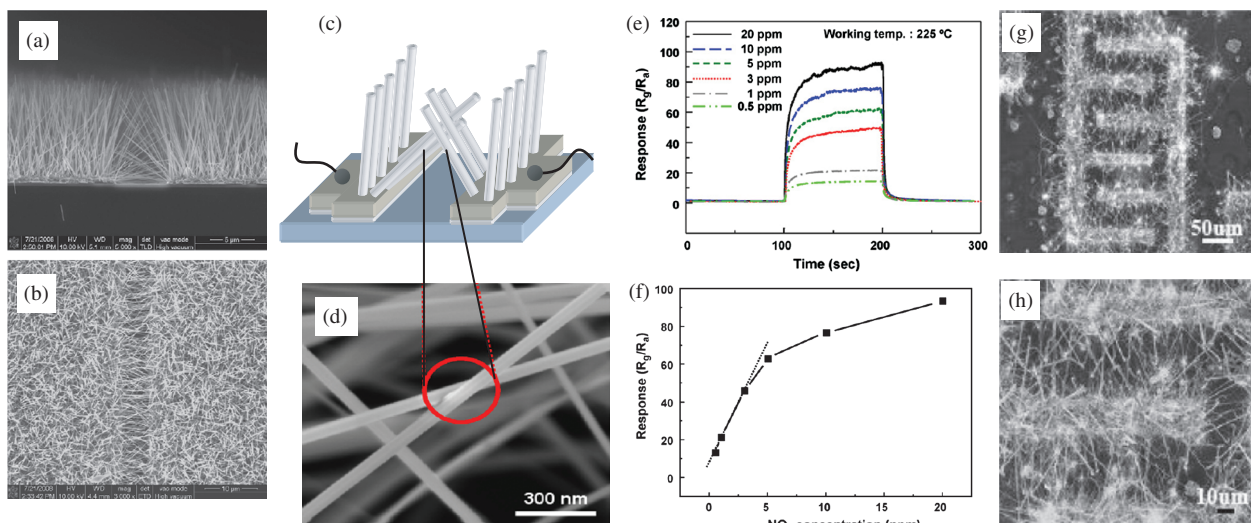


Fig. 3. (a) Side and (b) top-view SEM images clearly show selective growth of ZnO nanowires on Ti/Pt electrode. (c) The schematic illustration of ZnO-nanowire air bridges over the SiO₂/Si substrate. (d) The junction between ZnO nanowires grown on both electrodes. (e) Responses of a nanowire-bridge ZnO gas sensor as a function of NO₂ concentration (0.5–20 ppm) at operating temperature of 225 °C. (f) Response versus NO₂ concentration plot, which shows linear dependence in range of 0.5–3 ppm. (g–h) Nanowire with interconnecting network for bulk nanowire sensing. Figures 3(a–f) reprinted with permission from [59], M.-W. Ahn et al., *Sens. Actuators, B* 138, 168 (2009). © 2009, Elsevier Limited. Figures 3(g–h) reprinted with permission from [61], B. Wang et al., *J. Phys. Chem. C* 112, 6643 (2008). © 2008, American Chemical Society.

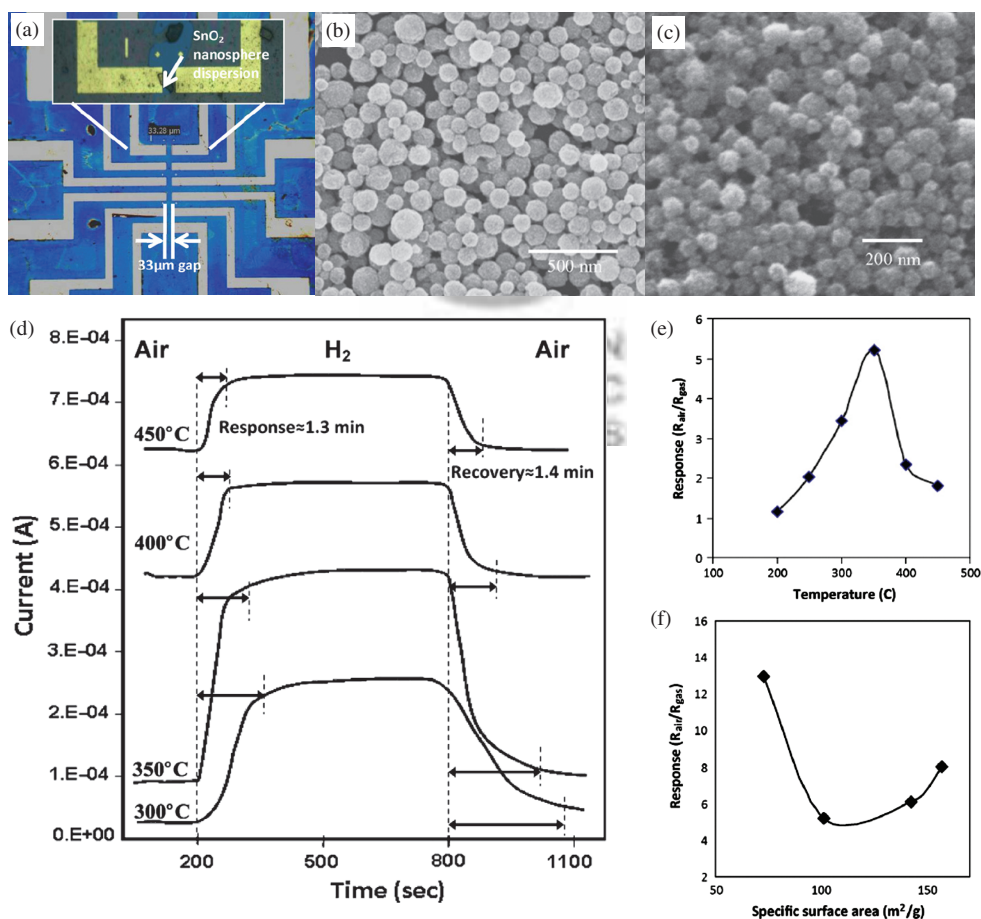


Fig. 4. (a) Optical image of the fabricated sensor. (b–c) SEM images of SnO₂ nanospheres synthesized at various reaction conditions. (d) Response and recovery times of the nanospheres sensor at various operating temperatures. Response plot versus (e) operating temperature and (f) specific surface area of SnO₂ nanospheres sensors. Reprinted with permission from [63], S. C. Yeow et al., *Sens. Actuators, B* 143, 295 (2009). © 2009, Elsevier Limited.

sensor at different operating temperatures (200–450 °C) are shown in Figure 4(e). As such, a higher operating temperature leads to a greater change in conductance and hence, greater response. On the other hand, desorption of all oxygen ionic species previously adsorbed occurs at high temperatures which explains the reduction in response as operating temperature is increased beyond the optimum value. Furthermore, the effect of specific surface area on the gas sensing performance is studied. Figure 4(f) shows the response plot obtained at 350 °C for all the samples with different specific surface areas. It can be observed that it is not a linear relationship. A possible explanation is that the inner surfaces of the porous nanospheres are not fully utilized for gas detection due to the limitation of diffusion of the analyte gas through the nanopores.

Sysoev et al. have reported thin film of nanoparticles and nanowires sensor mounted on microchip.⁶⁴ The device has demonstrated an excellent performance as a gas sensor capable of detecting and discriminating between several reducing gases in air at a ppb level of concentration. Both nanoparticles film and nanowire mats were deposited onto thermally oxidised SiO₂/Si substrates with Pt strip electrodes and Pt meander heaters microarray. The SnO₂ nanoparticles layers were deposited onto the substrates by spin-coating from an aqueous colloidal dispersion of the nanoparticles (Fig. 5(a)). SnO₂ nanowires are dry transferred to substrate to yield one-two monolayer network of percolating nanowires (Fig. 5(b)). Figures 5(c–d) depict the experimental data on a long-term evolution of

the SnO₂ nanostructures sensing characteristics toward the 2-propanol vapor. The response of nanowire mat to 1 ppm of 2-propanol is about ~6.4%. The as-prepared nanoparticles sensor exhibits a high response of $\sim 4 \times 10^3\%$. However, over 48 days, the nanoparticle response drops rapidly to 16%, close to the nanowires sensor capability. It has been postulated that the initial high porosity nanoparticles allow high gas diffusion thus rendering high response. Nevertheless, the long-term exposure to 2-propanol vapors at elevated operating temperature seems to facilitate sintering of nanoparticles. Thus, the two-terminal nanowire sensor is predicted to be a better conductometric gas sensor with relatively high gas sensitivity and long-term stability.

Other work on two terminal sensors is based on SnO₂ nanowires which were synthesized by thermal evaporation at 900 °C.⁶⁵ The obtained nanowires were doped with palladium by coating the nanowires with palladium chloride (PdCl₂) and annealed at 350 °C for 30 min in air in order to decompose PdCl₂ (Figs. 6(a–b)). Gas sensors based on undoped, 0.8 wt% Pd-doped, and 2 wt% Pd-doped SnO₂ nanowires were fabricated. These SnO₂ nanowire gas sensors showed a reversible response to H₂ gas at operating temperature of 150 °C (Figs. 6(c–d)). The sensor response increased with Pd concentration. The 2 wt% Pd-doped SnO₂ nanowire sensor showed a response as high as 253 for 1000 ppm H₂ gas at 100 °C (Fig. 6(d)). Pd doping has demonstrated to improve the sensor response and lower the operating temperature.

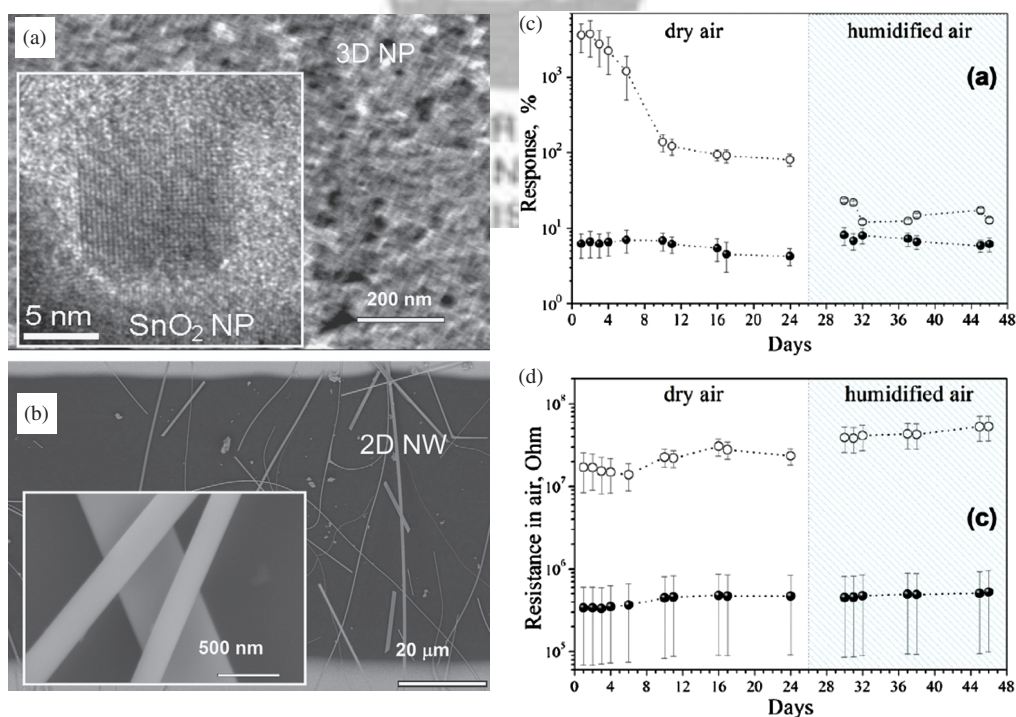


Fig. 5. HRTEM and SEM images of (a) SnO₂ mesoporous nanoparticles layer and (b) SnO₂ nanowires. (c) Response and (d) resistance of the nanoparticles (open circles) and nanowires (filled circles) over time. Reprinted with permission from [64], V. V. Sysoeva et al., *Sens. Actuators, B* 139, 699 (2009). © 2009, Elsevier Limited.

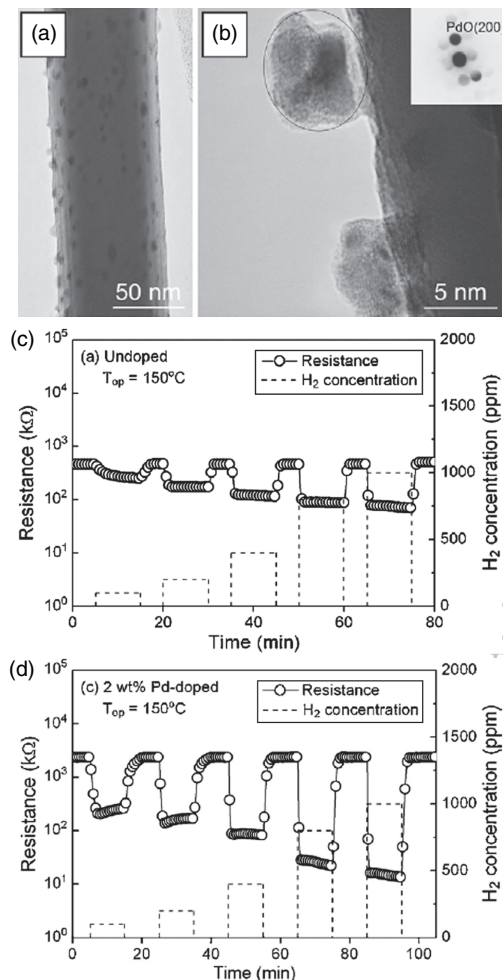


Fig. 6. (a–b) TEM image of a 2 wt% Pd-doped SnO_2 nanowire with a diameter of 80 nm. Inset shows the diffraction pattern of PdO nanoparticle on the nanowire. Changes in the resistance of (c) undoped and (d) 2 wt% Pd-doped SnO_2 nanowire gas sensors upon exposure to 100, 200, 400, 800 and 1000 ppm of H_2 gas. Reprinted with permission from [65], Y. B. Shen et al., *Sens. Actuators, B* 135, 524 (2009). © 2009, Elsevier Limited.

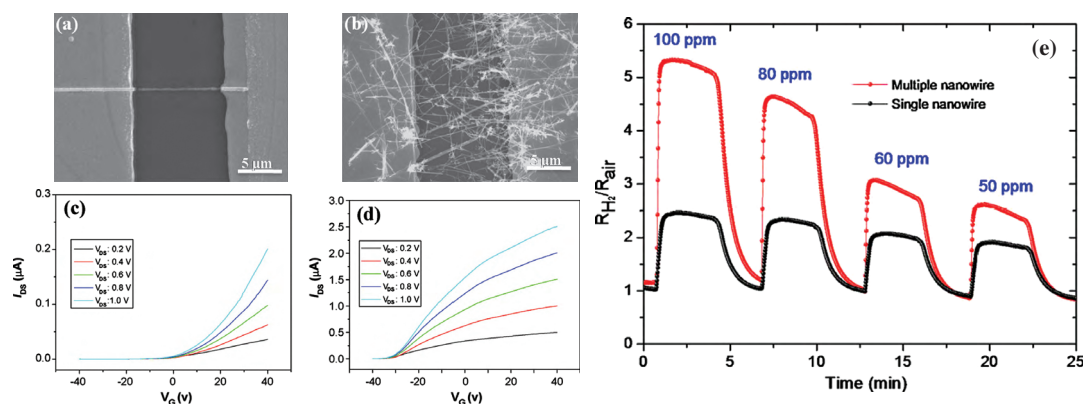


Fig. 7. (a–b) SEM images and (c–d) I - V curves of the single and multiple ZnO nanowire FETs, respectively. (e) The typical response curves of the single and multiple ZnO nanowire for variations of hydrogen concentration ranging from 50 to 100 ppm at 200 °C. Reprinted with permission from [67], R. Khan et al., *Sens. Actuators, B* 150, 389 (2010). © 2010, Elsevier Limited.

2.3. FET Nanostructure Sensor

In the case of field effect transistor sensor, active nanowire sensor element can act as a resistive element whose resistance can be changed by the field-effect or charge transfer process.^{66–69} The sensing properties can be monitored by varying the gate potential. For instance, Huang et al.⁶⁶ have reported a highly sensitive single Ga_2O_3 nanowire sensor which operates at room temperature although it is well-known fact that the Ga_2O_3 films sensors usually operate at high temperature of 400 to 1000 °C. The room temperature sensitivity observed here is most likely due to the good crystallinity and ultrahigh surface-to-volume ratios of the one-dimensional nanostructures. The gas-sensing measurements were performed for an individual Ga_2O_3 nanowire device with two Au/Ti electrodes and the source-drain biased voltage fixed at 10 V. When the individual Ga_2O_3 nanowire is exposed to a mixed flow of ammonia (1000 ppm) and air, the current is increased dramatically in the first 100 seconds and enhanced to about 30 times and stabilized at ~ 7800 nA. The Ga_2O_3 nanowire device exhibits a sensitivity of about 38 and a response time of ~ 58 s in the ambient of 1000 ppm air-diluted NH_3 .

Khan et al. have reported single and multiple nanowire FET sensors.⁶⁷ Figures 7(a and b) show typical SEM images of the single and multiple ZnO nanowire FET devices.⁷⁰ For comparison purposes, the distance between the electrodes and the diameter of the ZnO nanowires were kept the same for both devices. Figures 7(c and d) exhibited the typical electrical characteristics for the n -type single and multiple ZnO nanowire FETs respectively. The multiple nanowire devices showed greatly enhanced conductance due to increased number of nanowire. Figure 7(e) shows the gas sensing characteristics as a function of time for the single and multiple ZnO nanowires with various hydrogen concentrations in the range of 50–100 ppm at 200 °C. The sensor response was higher for the multiple

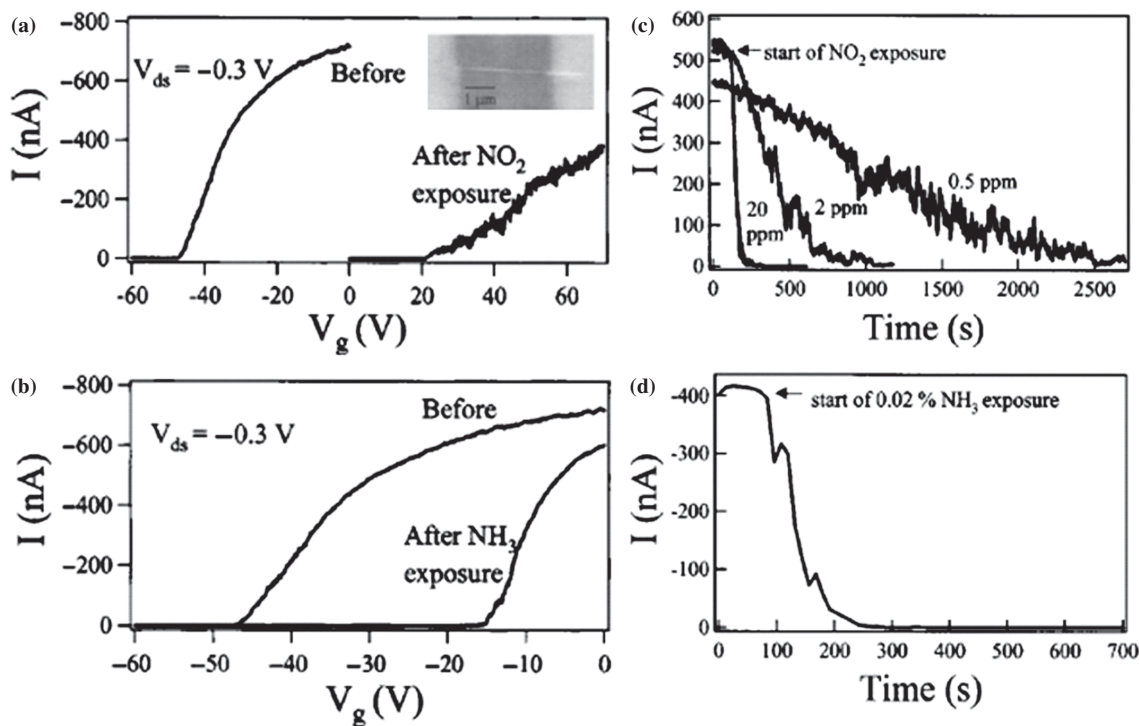


Fig. 8. $I-V_g$ curves before and after exposure to (a) 100-ppm NO_2 and (b) 1% NH_3 . The response time of (c) 20, 2, and 0.5 ppm NO_2 and (d) 0.02% NH_3 . Reprinted with permission from [68], C. Li et al., *Appl. Phys. Lett.* 82, 1613 (2003). © 2003, American Institute of Physics.

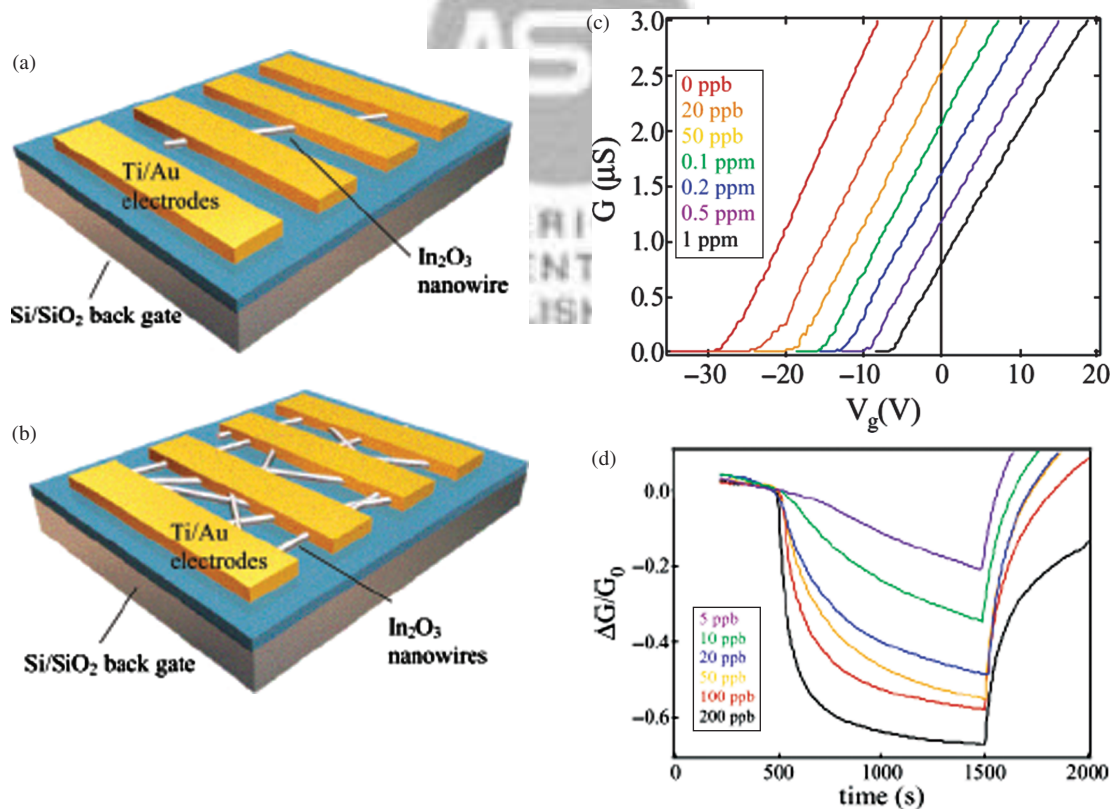


Fig. 9. Schematic of (a) single and (b) multiple nanowire transistor structure, where Ti/Au are deposited on nanowire-decorated Si/SiO_2 substrate as drain and source electrodes. (c) $I-V_g$ and (d) $\Delta G/G_0$ versus time for the single and multi nanowire sensor device recorded at different NO_2 concentrations. Reprinted with permission from [72], D. H. Zhang et al., *Nano Lett.* 4, 1919 (2004). © 2004, American Chemical Society.

ZnO nanowires than the response for the single ZnO nanowire over the entire range of hydrogen concentration. The multiple nanowires FET are made up of nanojunctions, which acted as a potential barrier for electron flow. The potential barrier decreased as the nanowire was exposed to the reducing gas, resulting in an increase in the current flow. The potential barrier modulation of multiple nanowires was more efficient than the modulation of the surface depletion of the single ZnO nanowire in gas sensing. Therefore, the potential barrier modulation in the nanojunctions caused the enhanced sensor response for the multiple nanowires.

Li et al.⁶⁸ demonstrated the use of a single one-dimensional nanowire FET sensor for high performance room temperature sensing. The sensor is made up of In_2O_3 nanowires of diameter 10 nm and length 5 μm which were placed between the source and drain electrodes with a silicon substrate as a back gate (Fig. 8 inset). The as-fabricated In_2O_3 nanowire sensor devices exhibited typical *n*-type transistor characteristics. The individual In_2O_3 nanowire transistors sensors exhibited superior performance as such the sensitivity is of 10^6 for NO_2 and 10^5 for NH_3 , which are four or five orders of magnitude better than results obtained from the thin-film based sensors.⁷¹ Response times are as short as 5 s for 100-ppm NO_2 and 10 s for 1% NH_3 . The lowest detectable gas concentrations are 0.5 ppm for NO_2 and 0.02% for NH_3 .

Furthermore, the sensing and selectivity between different gases can be studied by monitoring the current dependence on the gate bias and the threshold voltage shift, rendering a significant advantage over thin-film-based devices. Figure 8(a) shows two current–gate voltage (I – V_g) curves measured before and after exposure to 100 ppm NO_2 in argon with a constant source drain voltage (V_{ds}) of -0.3 V. Both measurements suggest that the In_2O_3 nanowires are *n*-type semiconductor as the conductance increase with gate bias. There is also a pronounced shift in the threshold voltage from -48 V before

the exposure to 20 V after the exposure. Adsorption of oxidizing gases reduces the number of free electrons in the *n*-type semiconductor and thus reduces the conductivity. Figure 8(b) shows two I – V_g curves before and after exposing to diluted NH_3 in Ar with $V_{ds} = -0.3$ V. A large threshold voltage shift from 248 V to 216 V is observed, with a maximum sensitivity of 105 at $V_g = -30$ V. For NO_2 concentrations of 20, 2, and 0.5 ppm, the response times are determined to be 20 s, 5 min and 10–12 min, respectively (Fig. 8(c)). Figure 8(d) shows a response time of about 2 min for 0.02% NH_3 which is the lowest tested concentration. The limitation is imposed by the availability of highly diluted NH_3 in air or argon.

Zhang et al.⁷² have demonstrated FET NO_2 sensor down to ppb levels based on both single and multiple In_2O_3 nanowires operating at room temperature as shown in schematic diagram Figures 9(a and b). Figure 9(c) shows the conductance versus gate bias (V_g) curves recorded in the six different NO_2 concentrations after exposure for 20 min for single nanowire FET. The threshold gate voltage shifted rightward monotonically with the increasing NO_2 /air concentration, implying the gradual suppression of carrier concentration of nanowire that scales linearly with the absolute value of gate threshold. As for the multi nanowire FET, the typical number of nanowires bridging adjacent metal electrodes is estimated to be 100–200. Figure 9(d) shows the sensing cycles of the multiwire FET device, corresponding to NO_2 /air concentrations of 5, 10, 20, 50, 100, and 200 ppb. The multiwire sensor showed a lower detection limit of 5 ppb, compared to the 20 ppb limit of single nanowire sensors. The room temperature detection limit is one of the lowest level ever reported. Furthermore, selective detection of NH_3 , O_2 , CO , and H_2 is possible with this nanowire FET sensor.

Kolmakov et al. has demonstrated an enhanced 1-D SnO_2 nanostructure-based sensor with and without Pd nanoparticles decorated nanobelts (Fig. 10(a)).⁷³ The deposited Pd works as catalysts for oxygen dissociation.

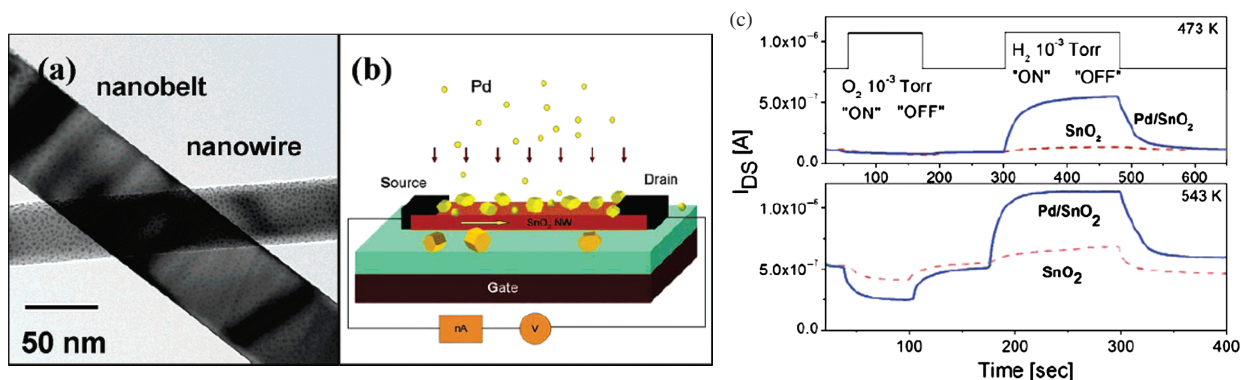


Fig. 10. (a) TEM of nanowires and nanobelts. (b) Schematic view of device used for the *in situ* conductometric measurements under gas exposure and metal deposition. (c) Response of a pristine (dashed line) and Pd-functionalized (solid line) nanostructure to sequential oxygen and hydrogen pulses at 473 K (top pane) and 543 K (bottom). Reprinted with permission from [73], A. Kolmakov et al., *Nano Nano Lett.* 5, 667 (2005). © 2005, American Chemical Society.

Figure 10(b) shows the schematic view of device used for the *in situ* conductometric FET measurements under gas exposure and metal deposition. The sensing performance of a SnO₂ nanowire toward sequential oxygen and hydrogen pulses at two different temperatures before (dashed curves) and after (solid curves) Pd deposition is shown in Figure 10(c). Functionalizing the nanowire surface with Pd leads to an enhancement in I_{DS} response for both gases and shorter response time. Functionalizing the nanowire surface with Pd leads to an enhancement in I_{DS} response for both gases and to an increased speed of response. Pd metal nanoparticles grown on reduced *n*-SnO₂ nanowires and nanobelts were found to form Schottky-barrier like junctions, which locally deplete the nanostructure of electrons. The improvements of sensitivity can be explained by the combined “spillover effect” of atomic oxygen formed catalytically on the Pd particles then migrating onto the tin oxide, and the back spillover effect in which weakly bound molecular oxygen migrate to the Pd and are catalytically dissociated. Raising the temperature raises the value of I_{DS} and shortens the response time of the sensor to O₂ and H₂. This effect is most prominent for oxygen for which the nanostructure only becomes activated above 543 K.

3. DIRECTED ASSEMBLY OF NANOSTRUCTURE SENSORS

The application of nanostructures as building blocks for sensor can be achieved by implementing effective assembly and integration techniques to transfer the nanostructures from growth substrates onto their respective device substrates. Several methods have been developed to assemble one-dimensional nanostructures which include microfluidic channel, Langmuir-Blodgett, blown bubble film, self-assembled monolayers, transfer printing alignment etc. In essence, these approaches employ external forces to align the nanostructures via wet or dry media. In some approaches, multilayer alignment is possible while others allow selective spatial alignment in large-scale. The development of nanostructures based sensor generally involves two processes. First, the assembly of nanostructures into highly integrated arrays with controlled orientation and spatial position; second, integration of interconnects between nanostructures and the micro or macroscopic subsystems.

3.1. Transfer Printed Nanostructure Sensor

Transfer printing is a dry alignment technique whereby nanostructures are printed in contact or close proximity to the substrate allowing the nanostructures to be aligned in the same direction and in a predetermined density. The nanostructures are grown on a substrate “stamps” and then stamped “printed” onto the receiving substrate.

The receiving substrate can have pre deposited electrodes upon which nanostructures can be aligned. The transfer printing deposition strategy has demonstrated to lead to well-defined and reproducible three-dimensional integrated circuits structures of controlled nanowires’ density and alignment over large substrate areas.^{74, 75}

Layer-by-layer assembly of nanowires for three-dimensional multifunctional electronics has been reported by Javey et al.⁷⁴ The dry alignment process involves (i) optimized growth of designed nanowires by nanocluster directed synthesis and (ii) patterned transfer of nanowires directly from a nanowire growth substrate to a second device substrate via contact printing (Figs. 11(a–b)).

In detail, a photolithographically patterned device substrate is first firmly attached to a bench top, and the nanowire growth substrate is placed face down in contact with the patterned device substrate. A gentle manual pressure is then applied from the top followed by sliding the growth substrate by 1–3 mm before the growth substrate is removed. Devices and circuits are then fabricated on the printed arrays of nanowires using conventional top-down lithography and metallization processes. To fabricate a three-dimensional FET, the contact printing of nanowires and device fabrication steps are repeated several times, along with the deposition of SiO₂ insulating layer, in order to obtain vertically stacked electronic layers (Figs. 11(c–d)). Another work which is also reported by the same group is ordered arrays of single-crystalline nano- and microwires of GaAs and InP with well-controlled lengths, widths, and shape have been fabricated over large areas from high quality bulk wafers by the use of traditional photolithography and anisotropic, chemical wet etching.⁷⁵ Printing using elastomeric stamps can transfer these wire arrays to plastic substrates, with excellent retention of order and crystallographic orientation of the wires. Figure 11(e) shows the various printing configuration; single to triple layers of nanowires patterns. Electrical measurements on simple test structures demonstrate the high degree of mechanical flexibility of the resulting wire arrays on plastics. The combination of top down wire fabrication and transfer printing represents an effective route to ultrahigh performance macroelectronic systems.

The nanowires are observed to be cleanly printed only at lithographically predefined locations FET device (Figs. 14(c–d)). The printed nanowires are aligned uniformly across mm or larger scale with relatively high densities (~4 nanowire/ μm). The monolithic integration of individual and parallel arrays of multifunctional and multilayer circuits consists of up to 10 addressable vertical layers. This alignment methodology is applicable for the wide range of nanowire materials, substrates and device designs. Furthermore, the simplicity and the low processing temperature requirement of the method makes it ideal for

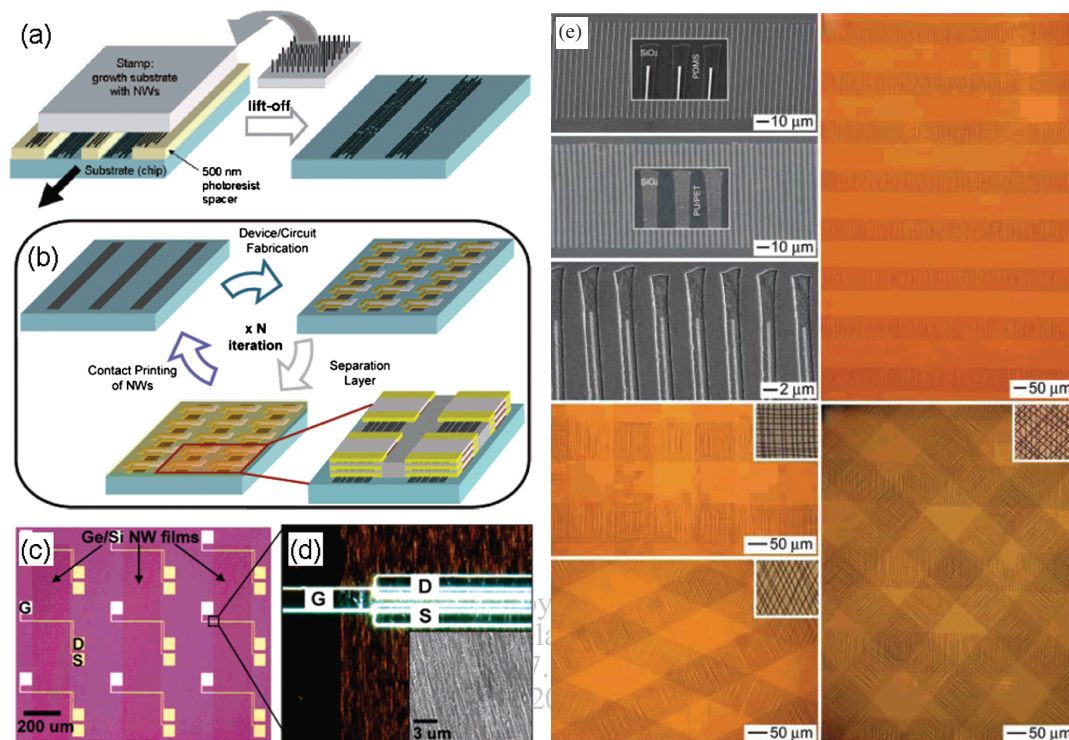


Fig. 11. Overview of 3D nanowire circuit integration. (a) Contact printing of nanowire from growth substrate to prepatterned substrate. (b) 3D nanowire circuit is fabricated by the iteration of the contact printing, device fabrication, and separation layer deposition steps. (c) Optical microscope image of 3D nanowire FETs. (d) Dark field image shows a parallel array of nanowires aligned between source (S), drain (D), and top gate (G) electrodes. Reprinted with permission from [74], A. Javey et al., *Nano Lett.* 7, 773 (2007). © 2007, American Chemical Society. (e) Images of single to multiple layers of GaAs wire array which are transfer printed using elastomeric stamps. Reprinted with permission from [75], Y. G. Sun and J. A. Rogers, *Nano Lett.* 4, 1953 (2004). © 2004, American Chemical Society.

achieving high performance three-dimensional integrated circuitry with different functionalities in distinct layers.

To demonstrate the potential of nanowire printing for large-area sensor integration, printed Si-nanowire arrays were configured as H_2 sensors. P-type SiNWs were printed on Si substrates, and two-terminal devices with Ni silicide contacts were fabricated.⁷⁷ The conductance of the Si nanowire array shows a strong dependence on the H_2 exposure, even at relatively low concentrations (250 ppm). It is worth noting that the nanowire printing method may provide a viable route toward the realization of electronic noses and smart sensors, capable of distinguishing chemical species while determining their concentrations. Such sensors may be envisioned through a large-scale integration of different sensor components interfaced with signal-processing functions. To achieve this goal, heterogeneous assembly of nanowire materials with orthogonal sensitivity to different analytes is needed, which may be achieved through a multistep nanowire printing process.

3.2. Dielectrophoretic Assembled Nanostructure Sensor

Dielectrophoresis (DEP) technique utilizes the dielectrophoretic force acting on the particles to induce spatial

movement when exposed to a non uniform electric field in the suspension medium. The force depends on a number of parameters such as the arrangement of the electrode, the frequency of the electric field and the resulting electric field distribution as well as the dielectric properties of the particles and the surrounding medium. By changing these factors, this force will pull the particle towards the higher electric field region (positive DEP effect) or push it towards the lower field region (negative DEP effect). DEP is a manipulation technique based on Maxwell's classical electromagnetic field theory to allow controlled movement of particles in a controlled electric field between the preset electrode structures. The DEP technique has demonstrated the potential for the construction of the nanosensors or nanoelectronic devices using as the nanostructured material as the building blocks.

Jiang et al.⁷⁸ have reported work on manipulation of ZnO nanorods by applying AC signals of suitable frequency and voltage to provide non uniform electrical field on different patterns of electrode (Figs. 12(a–b)). Similarly, Li et al.⁷⁹ have proposed DEP assembly of nanowires onto interdigitated microelectrodes (Fig. 12(c)) and mounted on micro-hotplate sensor platform (Fig. 12(d)).

Template-assisted electrodeposition method and a two-step thermal oxidation are employed. Through

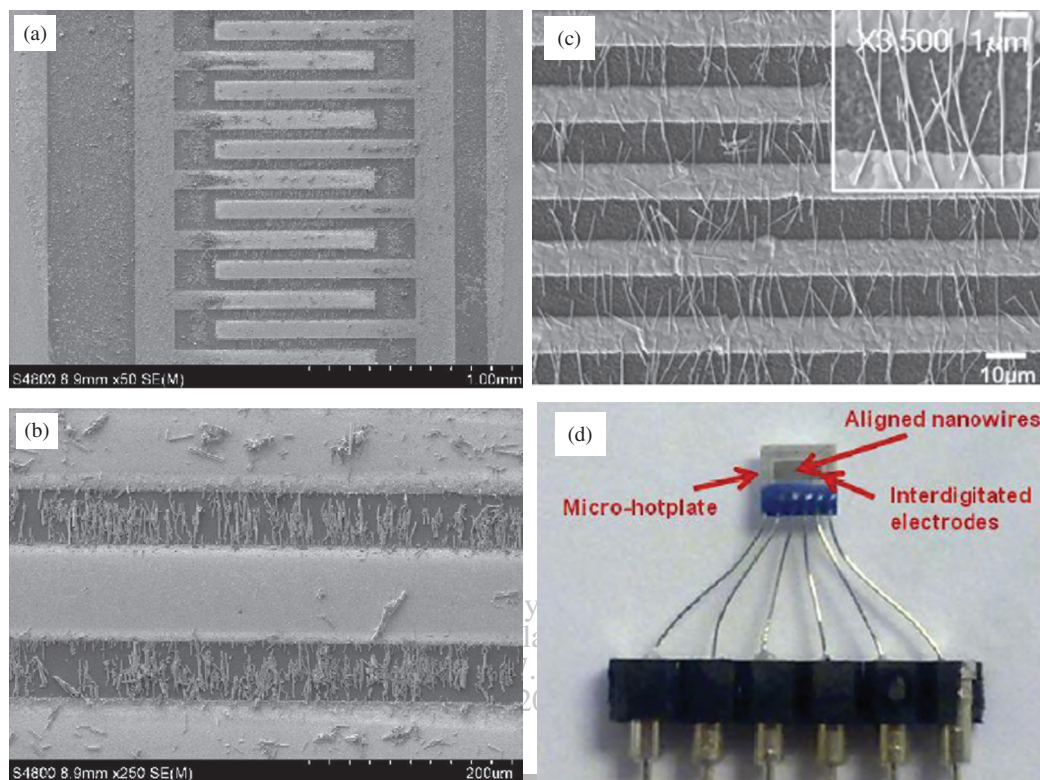


Fig. 12. (a–b) Low and high resolution SEM images of aligned ZnO nanowire in the interdigitated electrode array. The voltage and the frequency of the applied electric field are 10 V and 5 kHz. Reprinted with permission from [78], K. W. Jiang et al., *Sens. Actuators, B* 134, 79 (2008). © 2008, Elsevier Limited. (c) Well dispersed and fairly aligned indium/tin nanowires bridged across the electrode array. (d) Overview of the integrated sensor chip on micro-hotplate. Reprinted with permission from [79], X. P. Li et al., *Sens. Actuators, B* 148, 404 (2010). © 2008, Elsevier Limited.

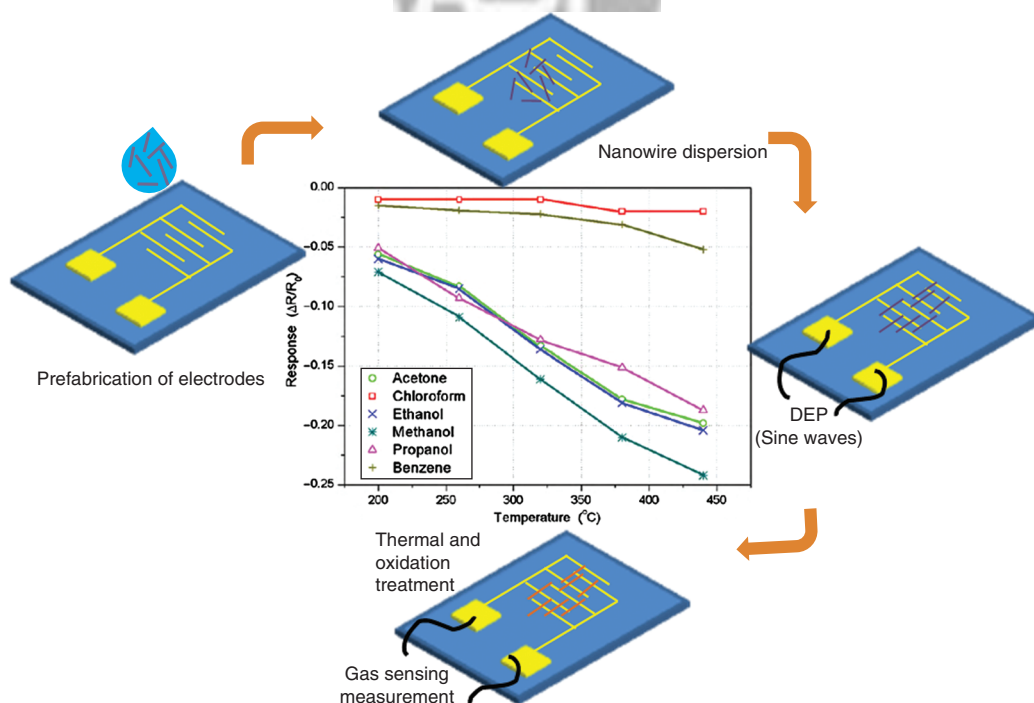


Fig. 13. Schematic of nanowire sensor integration: nanowire suspension drop casting on interdigitated microelectrodes; DEP assembly of metal nanowires; alignment of nanowires on microelectrodes; two-step thermal oxidation of nanowires and final integrated sensor chip. The response curve of the various volatile organic compounds versus temperature. Reprinted with permission from [80], T. Jinkawa et al., *J. Mol. Catal. A* 155, 193 (2000). © 2008, Elsevier Limited.

electrodeposition synthesis method, one-dimensional indium oxide, tin oxide, and indium–tin oxide nanowires were successfully fabricated. The nanowires are uniform and easy to process and assemble with good control of chemical compositions. The process flow of fabricating nanowire sensor via DEP alignment process is shown in Figure 13.⁸⁰ The nanowires solution is prepared and drop casted onto prefabricated interdigitated electrodes. The nanowires are observed to be randomly dispersed on the electrodes. The electrical field was generated by connecting a function generator to the interdigitated electrodes, while a sinusoidal wave with a frequency of 5–6 MHz and peak-to-peak voltage of 6 V was applied during the DEP process. At room temperature, ethanol volatilized within minutes, leaving nanowires aligned between the electrode pairs. Two thermal treatment processes were carried out after the DEP assembly of nanowires to lower the contact resistance between the aligned nanowires and microelectrodes and increased the stability of the nanowire assembled. First, aligned metal nanowires were heated to about 10 °C below their melting points; the temperature varied according to different material compositions. The bonding process was carried out in an inert nitrogen environment to prevent oxidation. Next, nanowires were heated at the temperature just below the melting point of the respective material in an atmospheric environment for 2 h. The temperature was later raised to 400–500 °C for another 3 h to achieve full oxidation. After the thermal and oxidation treatment, the nanowire sensor chip was ready for electrical measurement and chemical response

testing. The sensor was investigated with different volatile organic compounds. The sensitivity of three alcohols is the highest for methanol follow by ethanol, isopropanol. These findings coincide with the number of methyl groups in their chemical structure. Two competitive dissociative reactions were proposed⁸⁰ to explain the alcohol molecules adsorbed on the oxide surface, simply described as O–H and C–O bond-breaking processes, where the former one has a greater contribution to the resistance drop. The sensitivity order may relate to the preference of each chemical over these two competitive reactions.

4. NON-CONVENTIONAL SUBSTRATE SENSOR

Technological and industrial difficulties in further miniaturization of devices have called for innovative ways to incorporate gadgets into articles of everyday life. There are many sensors which have been fabricated on non conventional substrates, namely the plastic, textile and paper substrate sensor. The ability to fabricate sensor devices on plastic substrates is important owing to the demands of handheld, portable consumer electronics. Plastic substrates possess many attractive properties including biocompatibility, flexibility, light weight, shock resistance, softness and transparency. However, plastics has low melting point and they tend to deform or melt at temperatures of ~200 °C. This limits the synthesis temperature of nanostructures directly on the plastic substrate. Various ways to transfer the nanowires from donor substrate

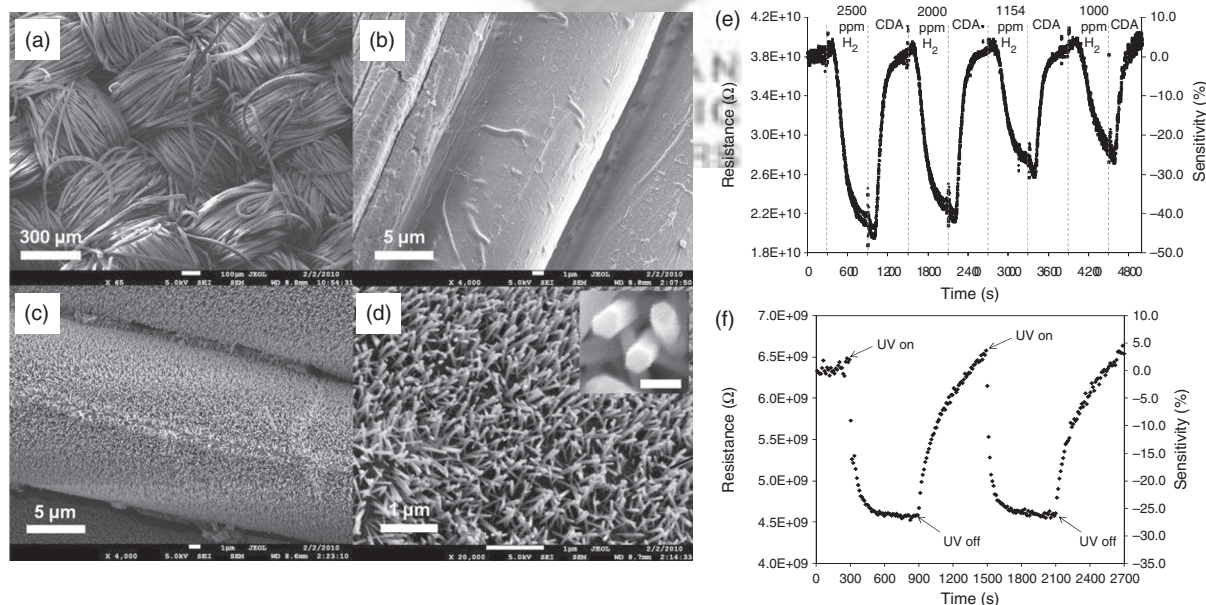


Fig. 14. SEM images of (a) cotton textile substrate in low magnification, (b) bare cotton fibres, (c) ZnO nanorods-coated cotton fibres and (d) high magnification images of ZnO nanorods on a cotton fibre. Scale bar in the inset represents 100 nm. Electrical responses of ZnO nanorods-on-cloth device to (e) various concentrations of H₂ gas and (f) UV irradiation. Clean dry air (CDA) was used to flush the chamber before and after each hydrogen injection. Experiments were performed in room temperature. Reprinted with permission from [89], Z. H. Lim et al., *Sens. Actuators, B* 151, 121 (2010). © 2010, Elsevier Limited.

to plastic substrate such as nanoimprint, contact transfer, Langmuir Blogett etc. have been developed. In addition, low temperature synthesis processes have also been developed to overcome this limitation. Mc Alpine et al. have reported plastic nanowire sensors based on Si nanowires which exhibit parts-per-billion sensitivity to NO_2 , a hazardous pollutant.⁸¹

Another type of non conventional substrate sensor is textile. Clothing is not only a necessity, it also encompasses a complete industry ranging from the down-to-earth basics to the upmarket and chic. Smart clothing/textiles are becoming very popular in the past decade. Smart textiles which have been developed include silicon flexible skins

and organic transistors on textile fibers.^{82,83} Another type of the smart sensing textiles which uses piezo-resistive properties has been developed. The approach for fabricating the fabrics was to coat a thin layer of piezo-resistive materials, such as polypyrrole or a mixture of rubbers and carbons, on conventional fabrics to form fabric-based sensors.⁸⁴⁻⁸⁶ The function of the developed sensors is similar to that of flexible strain gauges which can measure strains when they are subjected to a tensile stress. Other innovations which are not actively explored are textiles which can detect environmental conditions, which then react and adapt to environmental changes. Furthermore, smart textiles can be made to measure and monitor the physiological conditions

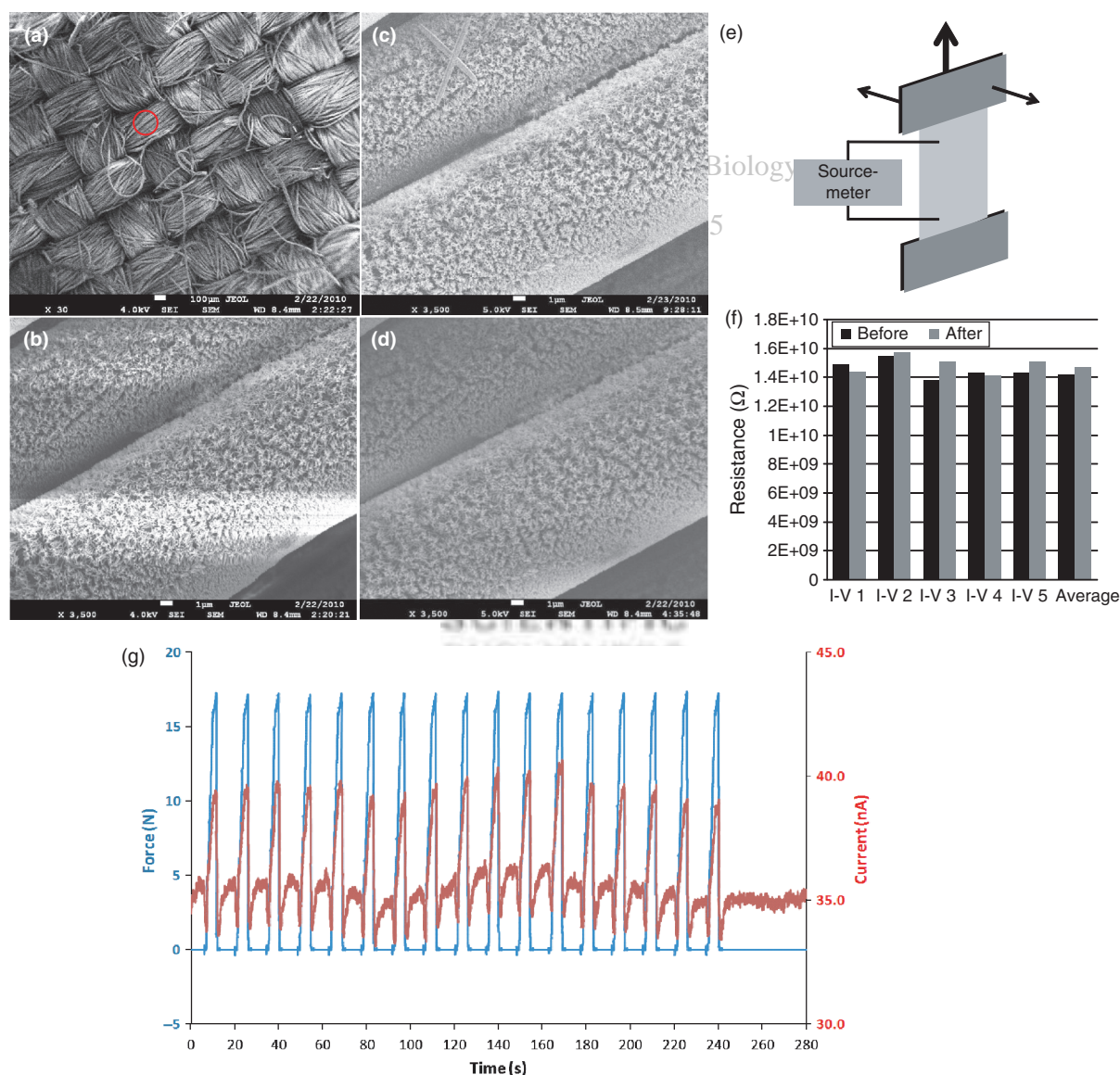


Fig. 15. SEM images of (a) low resolution ZnO-nanorods-coated textile with selected area (circled in red) for subsequent studies (b) the selected ZnO nanorods-coated yarns before stretching, twisting and sonication, (c) the same yarns after repeated stretching and twisting and (d) 5 minutes of water sonification. (e) Schematic diagram of the electro-mechanical testing and (f) electrical properties before and after each stretching and twisting cycle. (g) Electrical measurement of ZnO nanorods-on-cloth device while subjected to controlled stress cycles with a mechanical testing system. Reprinted with permission from [89], Z. H. Lim et al., *Sens. Actuators, B* 151, 121 (2010). © 2010, Elsevier Limited.

of the wearer e.g., perspiration, heartbeat etc. Thus they can be applied various healthcare systems.

4.1. Textile Sensor

While the development of wearable devices has been reported, the incorporation of nano-materials into the designs has not been well explored. In addition, problems such as complex process, mass production, washability, and wearing comforts needs to be well addressed. The ease of synthesizing ZnO nanowires or nanorods on almost any substrates welcomes large-scale incorporation on textile. ZnO nano-structures are believed to be non-toxic and bio-safe,⁸⁷ allowing their direct usage in daily applications. While the use of nano-materials in daily human activities raised questions on its potential health risks, there is to date no *in vivo* evidence of toxicity of nano-particulate ZnO.⁸⁸

SEM images of the textile and nanorods displayed in Figures 14(a–d) show radially oriented nanorods (diameter ~ 80 nm) with hexagonal cross-section grown along the cylindrical fibres (diameter $\sim 15 \mu\text{m}$).⁸⁹ Length of the nanorods is $\sim 1 \mu\text{m}$. The nanorods form a uniform and dense coverage around entire lengths of the fibres to form a cross-linked semi-conductive textile.

The conductive textile shows excellent multiple sensing (gas and optical) performances at room temperature as shown in Figures 14(e) and (f) respectively. In the presence of hydrogen gas, chemisorbed oxygen ions are reduced to release electrons to the conduction band of the ZnO surface resulting in an increase in conductivity. In addition, the reduction reaction decreases the surface density of the oxygen adsorbate, leading to a reduction in the width of the depletion region and the height of the surface potential barrier, thus resulting in the decrease in the resistance of the sensor. The mechanism for UV sensing

Delivered by Ingenta to:

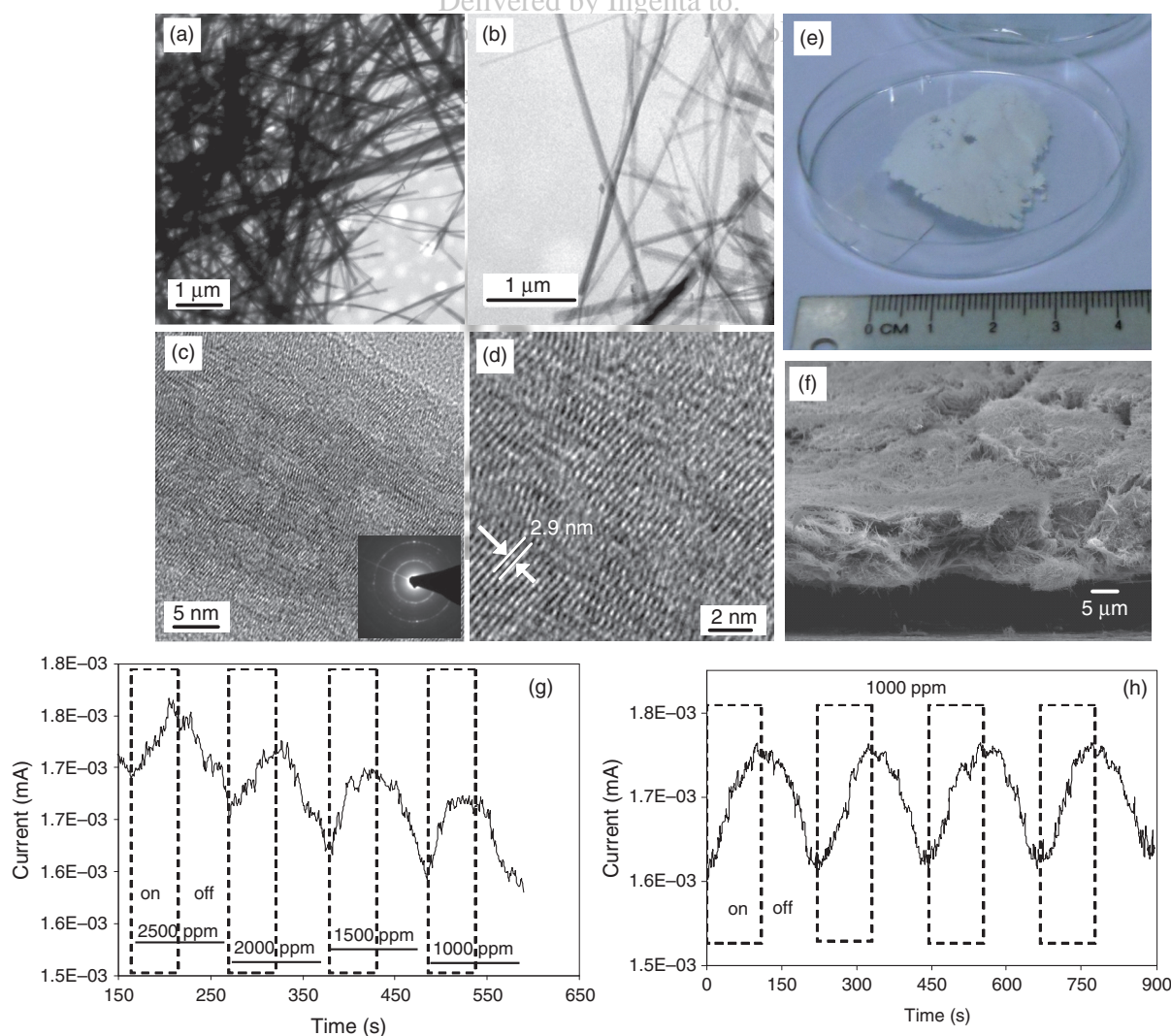


Fig. 16. (a–b) Low and (c–d) high resolution TEM images of the nanobelts. (e) Image of nanobelts sheet made without any addition of binder or reinforcement chemicals. (f) Cross-sectional SEM image of the nanobelts sheet. Current response of the sensor at (g) varying and (h) same ppm H_2 concentration. Reprinted with permission from [90], S. Bela et al., *J. Phys. D: Appl. Phys.* 43, 35401 (2010). © 2010, Institute of Physics.

is similar to that of hydrogen sensing, with holes from the photo-generated electron-hole pairs playing the role of removing the adsorbed oxygen molecules instead.

A notable feature of the ZnO nanorods-coated textile device is its fine morphological and electrical stability under multiple stress and washing cycles. A critical challenge of semi-conductive yarns and textile is its durability and constancy of electrical performance. SEM analyses (Figs. 15(a-d)) of the nanorods -on-cloth before and after stretching, twisting and ashing cycles show no cracks or delamination of the nanorods from the fibres respectively. Figure 15(e) shows a schematic of the electro-mechanical testing. Electrical characterisations made before and after each stretching and twisting cycle (Fig. 15(f)) show good electrical stability. We further perform electrical conductivity measurements while stretching and relaxing the textile device in a controlled manner. The semiconducting textile exhibits a higher conductivity when stretched due to tighter packing (increased contact junctions) of the ZnO nanorods-coated fibers. Figure 15(g) shows the variation of current through the textile device as it underwent repeated cycles of stress and relaxation. When the stress is released, conductivity falls and stabilises to the original state. Again the morphology of the nanorods-on-textile suffered no cracks of delamination or noticeable degradation after the electromechanical testing.

4.2. Free Standing Sheet Sensor

Another non conventional sensor substrate is a free standing sheet of nanowire paper. The nanostructures are to be produced in gram quantities so that it can be easily made into nanostructured paper sheet. The thickness of the nanostructures sheet can be tuned according to the amount of nanostructures used. After the filtering was completed, a sheet of nanostructures was formed by sandwiching between a metal calender which was pressed and heated to ensure the nanowires are well dried and bonded together to form the free-standing paper.

Bela et al. have been reported synthesis of hybrid titanate and titania nanobelts (Figs. 16(a-d)) in a large-scale quantity for gas sensing applications.⁹⁰ The nanobelts are synthesized from TiO_2 powder based on hydrolysis and ion exchange of NaOH base and HCl acid respectively. Sheets of as-synthesized nanobelts are used for electrical and gas sensing measurements. Figure 16(e) shows the white nanobelts sheet made without any addition of binder or reinforcement chemicals. Cross-sectional SEM image of Figure 16(f) shows that the nanobelts sheet has a thickness of $\sim 15 \mu\text{m}$. Figures 16(g and h) show the current response of the sensor at varying and same ppm H_2 concentrations respectively. The measurements were conducted at an operating temperature of 300°C . From the graphs, it is evident that the introduction of hydrogen causes the resistance of the sensor to reduce because of the injection of electrons

onto the surface of the metal-oxide nanostructures, thereby improving the conductivity of the bulk sensing capabilities. The resistance increases as the concentration of H_2 is varied from 2500 to 1000 ppm. The response time (90% of $R_{\text{air}} - R_{\text{gas}}$) is achieved within the first 40–50 s while the recovery time is 1.0–1.2 min. From the Figure 7(c), it was observed that the sensing response was rather stable and reversible. In oxidizing atmosphere of 300°C , ambient oxygen is adsorbed on the surface of nanobelts most likely with a negative charge. Subsequently, with the introduction of a reducing H_2 gas, it reacts with the negatively charged surface oxygen and decreases the resistance by the injection of electron.

5. CONCLUSIONS

There is an immense technological and scientific potentials of nanostructured materials in nanodevice applications, and already numerous nanomaterial based sensors using various materials have been reported. These oxide materials can be synthesized by various synthetic routes which include both physical and chemical methods. The potential application of these nanostructures as sensor depends greatly on the ability to precisely control their dimension, chemical composition, surface property, phase purity, and crystal structure. Sensor of various configurations; bulk, two-terminal and FET device have been fabricated. The integrability of the nanostructure sensor into microelectronic fabrication technology is an issue that needs to be addressed. Various ways to assemble nanowires so as to ease the device fabrication process have been developed. The recent advances in assembling larger and more complex nanowire sensor arrays and integrating them into nanoscale, electronics can lead to exquisite sensor system performances. These sensory systems can sensitively transduce gas/chemical/biological binding events into electronic/digital signals which promise a sophisticated nano-electronics sensing system.

6. FUTURE DIRECTIONS

Although nanomaterial based sensors are expected to outperform their bulk component, there are still many issues and parameters to be studied and addressed. Parameters to be explored include structural and composition tuning as well as doping and functionalization of surfaces to increase selectivity, sensitivity and materials integrity for long-term stability. Other parameters such as limits of detection, limits of quantification, dynamic range, response and recovery times and lifetime have to be studied and improved as well. The long-term reliability of a sensor is important since progressive drifts in the characteristics and/or responses of the sensors affect accurate testing and analysis. The drift of the sensors are frequently related to high working temperatures and exposure to chemically active

ambient gas. Many other issues include aging, grain-size growth, poisoning due to unknown chemical species, diffusion processes within the device etc. are to be addressed as well.

The future direction of the solid-state gas sensor is towards integrated wireless/remote, multi-purpose sensing, high selectivity recognition of a specific biological or chemical species with “electronic-nose-tongue” capabilities. In addition, development of miniaturized analytical sensor which can be integrated in-line or/and as standalone portable sensors is paramount for industrial applications. The sensors can further be refined into a network of sensor arrays providing rapid screening, monitoring and reporting system. The data are collected in a database and form part of a feedback guidance system to the control algorithm in industrial processes.

Acknowledgments: The work is supported by National University of Singapore, grant R-263-000-532-112. Images used for the cover page are kindly contributed by Z. H. Lee and M. Kevin, multidisciplinary laboratory.

References and Notes

- D. James, S. M. Scott, Z. Ali, and W. T. O'Hare, *Microchim. Acta* **149**, 1 (2005).
- C.-D. Kohlin, *Nanoelectronics and Information Technology*, edited by R. Waser, Wiley-VCH, Berlin (2005), p. 851.
- M. E. Franke, T. J. Koplin, and U. Simon, *Small* **2**, 36 (2006).
- A. Kolmakov and M. Moskovits, *Annu. Rev. Mater. Res.* **34**, 151 (2004).
- A. Mandelis and C. Christofides, *Physics, Chemistry and Technology of Solid State Gas Sensor Devices*, Wiley-Interscience, New York (1993).
- P. T. Moseley, *Sens. Actuators, B* **6**, 149 (1992).
- N. M. White and J. D. Turner, *Meas. Sci. Technol.* **8**, 1 (1997).
- D. Kohl, *J. Phys. D* **34**, R125 (2001).
- N. Pinna, G. Neri, M. Antonietti, and M. Niederberger, *Angew. Chem. Int. Ed.* **43**, 4345 (2004).
- L. P. Sun, L. H. Huo, H. Zhao, S. Gao, and J. G. Zhao, *Sens. Actuators, B* **114**, 387 (2006).
- Z. F. Liu, T. Yamazaki, Y. B. Shen, T. Kikuta, N. Nakatani, and Y. X. Li, *Sens. Actuators, B* **129**, 666 (2008).
- C. S. Rout, A. R. Raju, A. Govindaraj, and C. N. R. Rao, *J. Nanosci. Nanotechnol.* **7**, 1923 (2007).
- M. S. Arnold, P. Avouris, Z. W. Pan, and Z. L. Wang, *J. Phys. Chem. B* **107**, 659 (2003).
- I. Jimenez, I. M. A. Centeno, R. Scotti, F. Morazzoni, A. Cornet, and J. R. Morante, *J. Electrochem. Soc.* **150**, H72 (2003).
- S. Semancik and R. E. Cavicchi, *Thin Solid Films* **206**, 81 (1991).
- N. S. Baik, G. Sakai, N. Miura, and N. Yamazoe, *Sens. Actuators, B* **63**, 74 (2000).
- M. Ivanovskaya, P. Bogdanov, G. Faglia, and G. Sberveglieri, *Sens. Actuators, B* **68**, 344 (2000).
- K. Ihokura and I. Watson, *The Stannic Oxide Gas Sensor—Principles and Applications*, CRC Press, Boca Raton (1994).
- K. D. Schierbaum, U. Weimar, and W. Gopel, *Sens. Actuators, B* **7**, 1 (1992).
- G. Korotcenkov, *Sens. Actuators, B* **121**, 664 (2007).
- J. G. Lu, P. C. Chang, and Z. Y. Fan, *Mater. Sci. Eng.* **52**, 49 (2006).
- T. Yamamoto and H. Katayama-Yoshida, *Jpn. J. Appl. Phys.* **38**, L166 (1999).
- J. G. Lu, L. P. Zhu, Z. Z. Ye, F. Zhuge, B. H. Zhao, D. W. Ma, L. Wang, and J. Y. Huang, *J. Mater. Sci.* **41**, 467 (2006).
- J. Zhong, S. Muthukumar, Y. Chen, Y. Lu, H. M. Ng, W. Jiang, and E. L. Garfunkel, *Appl. Phys. Lett.* **83**, 3401 (2003).
- S. Y. Bae, C. W. Na, J. H. Kang, and J. Park, *J. Phys. Chem. B* **109**, 2526 (2005).
- S. Y. Li, P. Lin, C. Y. Lee, T. Y. Tseng, and C. J. Huang, *J. Phys. D: Appl. Phys.* **37**, 2274 (2004).
- D. K. Hwang, H. S. Kim, J. H. Lim, J. Y. Oh, J. H. Yang, S. J. Park, K. K. Kim, D. C. Look, and Y. S. Park, *Appl. Phys. Lett.* **86**, 151917 (2005).
- W. Lee, M. C. Jeong, S. W. Joo, and J. M. Myoung, *Nanotechnology* **16**, 764 (2005).
- W. Lee, M. C. Jeong, and J. M. Myoung, *Appl. Phys. Lett.* **85**, 6167 (2004).
- D. W. Zeng, C. S. Xie, B. L. Zhu, R. Jiang, X. Chen, W. L. Song, J. B. Wang, and J. Shi, *J. Cryst. Growth* **266**, 511 (2004).
- G. Z. Shen, J. H. Cho, J. K. Yoo, G. C. Yi, and C. J. Lee, *J. Phys. Chem. B* **109**, 5491 (2005).
- J. B. Cui and U. J. Gibson, *Appl. Phys. Lett.* **87**, 133108 (2005).
- C. X. Xu, X. W. Sun, Z. L. Dong, M. B. Yu, Y. Z. Xiong, and J. S. Chen, *Appl. Phys. Lett.* **86**, 173110 (2005).
- D. A. Schwartz, K. R. Kittilstved, and D. R. Gamelin, *Appl. Phys. Lett.* **85**, 1395 (2004).
- C. Ronning, P. X. Gao, Y. Ding, Z. L. Wang, and D. Schwen, *Appl. Phys. Lett.* **84**, 783 (2004).
- A. J. Mieszawska, R. Jalilian, G. U. Sumanasekera, and F. P. Zamborini, *Small* **3**, 722 (2007).
- B. Zhu, K. Li, S. Zhang, S. Wu, and W. Huang, *Prog. Chem.* **20**, 48 (2008).
- J. X. Wang, S. S. Xie, and W. Zhou, *MRS Bull.* **32**, 123 (2007).
- W. Lu and C. M. Lieber, *J. Phys. D: Appl. Phys.* **39**, R387 (2006).
- X. Wang and Y. D. Li, *Inorganic Chemistry* **45**, 7522 (2006).
- Y. Shen, T. Yamazaki, Z. Liu, D. Meng, T. Kikuta, N. Nakatani, M. Saito, and M. Mori, *Sens. Actuators B* **135**, 524 (2009).
- A. Kolmakov, Y. Zhang, G. Cheng, and M. Moskovits, *Adv. Mater.* **15**, 997 (2003).
- X. T. Zhou, J. Q. Hu, C. P. Li, D. D. D. Ma, C. S. Lee, and S. T. Lee, *Chem. Phys. Lett.* **369**, 220 (2003).
- T.-J. Hsueh, C.-L. Hsu, S.-J. Chang, and I.-C. Chen, *Sens. Actuators, B* **126**, 473 (2007).
- Q. Wan, Q. H. Li, Y. J. Chen, T. H. Wang, X. L. He, J. P. Li, and C. L. Lin, *Appl. Phys. Lett.* **84**, 3654 (2004).
- G. J. Li, X. H. Zhang, and S. Kawi, *Sens. Actuators B* **60**, 64 (1999).
- G. J. Li and S. Kawi, *Talanta* **45**, 759 (1998).
- E. T. H. Tan, G. W. Ho, A. S. W. Wong, S. Kawi, and A. T. S. Wee, *Nanotechnology* **19**, 255706 (2008).
- S. Luo, G. Fu, H. Chen, and Y. Zhang, *Mater. Chem. Phys.* **109**, 541 (2008).
- C. Y. Wang, M. Ali, T. Kups, C. C. Roehlig, V. Cimalla, T. Stauden, and O. Ambacher, *Sens. Actuators, B* **130**, 589 (2008).
- J. Ahmed, S. Vaidya, T. Ahmad, P. Sujatha Devi, D. Das, and A. K. Ashok, *Mater. Res. Bull.* **43**, 264 (2008).
- J. Kaur, R. Kumar, and M. C. Bhatnagar, *Sens. Actuators, B* **126**, 478 (2007).
- D. Lusic, M. Strand, A. Lloyd-Spetz, K. Buchholt, E. Ieva, P. O. Kall, and M. Sanati, *Top. Cata.* **45**, 105 (2007).
- A. Teleki, S. E. Pratsinis, K. Kalyanasundaram, and P. I. Gouma, *Sens. Actuators, B* **119**, 683 (2006).
- X. L. Gou, G. X. Wang, X. Y. Kong, D. Wexler, J. Horvat, J. Yang, and J. Park, *Chem. Eur. J.* **14**, 5996 (2008).
- X. Feng, Z. J. Li, P. Y. Wang, and Y. F. Zhou, *J. Mat. Sci.* **40**, 6597 (2005).
- J. Chen, L. Xu, W. Li, and X. Gou, *Adv. Mater.* **17**, 582 (2005).
- Z. B. Zhuang, Q. Peng, J. F. Liu, X. Wang, and Y. D. Li, *Inorg. Chem.* **46**, 5179 (2007).

59. M.-W. Ahn, K.-S. Park, J.-H. Heo, D.-W. Kim, K. J. Choi, and J.-G. Park, *Sens. Actuators B* 138, 168 (2009).
60. H. T. Wang, B. S. Kang, F. Ren, L. C. Tien, P. W. Sadik, D. P. Norton, S. J. Pearton, and J. Lin, *Appl. Phys. A* 81, 1117 (2005).
61. B. Wang, L. F. Zhu, Y. H. Yang, N. S. Xu, and G. W. Yang, *J. Phys. Chem. C* 112, 6643 (2008).
62. T. H. Jung, S.-I. Kwon, J.-H. Park, D.-G. Lim, Y.-J. Choi, and J.-G. Park, *Appl. Phys. A* 91, 707 (2008).
63. S. C. Yeow, W. L. Ong, A. S. W. Wong, and G. W. Ho, *Sens. Actuators B* 143, 295 (2009).
64. V. V. Sysoeva, T. Schneiderb, J. Goschnickb, I. Kiselevb, W. Habichtb, H. Hahn, E. Strelcovc, and A. Kolmakov, *Sens. Actuators B* 139, 699 (2009).
65. Y. B. Shen, T. Yamazaki, Z. F. Liu, D. Meng, T. Kikuta, N. Nakatani, M. Saito, and M. Mori, *Sens. Actuators B* 135, 524 (2009).
66. Y. Huang, S. Yue, Z. Wang, Q. Wang, C. Shi, Z. Xu, X. D. Bai, C. Tang, and C. Gu, *J. Phys. Chem. B* 110, 796 (2006).
67. R. Khan, H.-W. Ra, J. T. Kim, W. S. Jang, D. Sharma, and Y. H. Im, *Sens. Actuators B* 150, 389 (2010).
68. C. Li, D. H. Zhang, X. L. Liu, S. Han, T. Tang, J. Han, and C. Zhou, *Appl. Phys. Lett.* 82, 1613 (2003).
69. Z. Fan and J. G. Lu, *Appl. Phys. Lett.* 86, 123510 (2005).
70. Z. Y. Fan, D. W. Wang, P. C. Chang, W. Y. Tseng, and J. G. Lu, *Appl. Phys. Lett.* 85, 5923 (2004).
71. M. Liess, *Thin Solid Films* 410, 183 (2002).
72. D. H. Zhang, Z. Q. Liu, C. Li, T. Tang, X. L. Liu, S. Han, B. Lei, and C. W. Zhou, *Nano Lett.* 4, 1919 (2004).
73. A. Kolmakov, D. O. Klenov, Y. Lilach, S. Stemmer, and M. Moskovits, *Nano Lett.* 5, 667 (2005).
74. A. Javey, S. W. Nam, R. S. Friedman, H. Yan, and C. M. Lieber, *Nano Lett.* 7, 773 (2007).
75. Y. G. Sun and J. A. Rogers, *Nano Lett.* 4, 1953 (2004).
76. Z. Fan, J. C. Ho, Z. A. Jacobson, R. Yerushalmi, R. L. Alley, H. Razavi, and A. Javey, *Nano Lett.* 8, 20 (2008).
77. Z. Y. Fan, J. C. Ho, T. Takahashi, R. Yerushalmi, K. Takei, A. C. Ford, Y.-L. Chueh, and A. Javey, *Adv. Mater.* 21, 3730 (2009).
78. K. W. Jiang, W. J. Liu, L. J. Wan, and J. Zhang, *Sens. Actuators B* 134, 79 (2008).
79. X. P. Li, E. China, H. W. Sun, P. Kurup, and Z. Y. Gu, *Sens. Actuators B* 148, 404 (2010).
80. T. Jinkawa, G. Sakai, J. Tamaki, N. Miura, and N. Yamazoe, *J. Mol. Catal. A* 155, 193 (2000).
81. M. C. McAlpine, H. Ahmad, D. W. Wang, and J. R. Heath, *Nat. Mater.* 6, 379 (2007).
82. R. B. Katragadda and Y. Xu, A Novel Intelligent Textile Technology Based on Silicon Flexible Skins, Electrical and Computer Engineering, Wayne State University, Detroit, Michigan, USA, ISWC (2005), pp. 78–81.
83. J. B. Lee and V. Subramanian, *IEEE Trans. Electron Devices* 62, 269 (2005).
84. R. Wijesiriwardana, K. Mitcham, and T. Dias, Fibre-meshed transducers based real time wearable physiological information monitoring system, *Proceedings of the 8th International Symposium on Wearable Computers, ISWC'04* (2004), pp. 40–47.
85. R. Wijesiriwardana, *IEEE Sens. J.* 6, 571 (2006).
86. E. P. Scilingo, F. Lorussi, A. Mazzoldi, and D. De Rossi, *Sens. J. IEEE* 3, 460 (2003).
87. J. Zhou, N. Xu, and Z. L. Wang, *Adv. Mater.* 18, 2432 (2006).
88. G. J. Nohynek, E. K. Dudour, and M. S. Roberts, *Nanotechnology* 21, 136 (2008).
89. Z. H. Lim, Z. X. Chia, M. Kevin, A. S. W. Wong, and G. W. Ho, *Sens. Actuators B* 151, 121 (2010).
90. S. Bela, A. S. W. Wong, and G. W. Ho, *J. Phys. D: Appl. Phys.* 43, 35401 (2010).

Received: 4 November 2010. Accepted: 20 January 2011.

